

Magnetization relaxation in the single molecule magnet Ni₄ under continuous microwave irradiation

G. DE LOUBENS¹, D. A. GARANIN², C. C. BEEDLE³, D. N. HENDRICKSON³ and A. D. KENT¹

¹ *Department of Physics, New York University, 4 Washington Place, New York, New York 10003, USA*

² *Department of Physics and Astronomy, City University of New York, 250 Bedford Park Boulevard West, Bronx, New York 10468-1589, USA*

³ *Department of Chemistry and Biochemistry, University of California San Diego, La Jolla, California 92093, USA*

PACS 75.45.+j – Macroscopic quantum phenomena in magnetic systems

PACS 75.50.Xx – Molecular magnets

PACS 76.30.-v – Electron paramagnetic resonance and relaxation

Abstract. - Spin relaxation between the two lowest-lying spin-states has been studied in the $S = 4$ single molecule magnet Ni₄ under steady state conditions of low amplitude and continuous microwave irradiation. The relaxation rate was determined as a function of temperature at two frequencies, 10 and 27.8 GHz, by simultaneously measuring the magnetization and the absorbed microwave power. A strong temperature dependence is observed below 1.5 K, which is not consistent with a direct single-spin-phonon relaxation process. The data instead suggest that the spin relaxation is dominated by a phonon bottleneck at low temperatures and occurs by an Orbach mechanism involving excited spin-levels at higher temperatures. Experimental results are compared with detailed calculations of the relaxation rate using the universal density matrix equation.

Quantum tunneling of magnetization (QTM) [1, 2] and quantum phase interference [3, 4] have been intensively studied in single molecule magnets (SMMs). These materials have also been suggested as candidates for qubits in quantum processors [5] and for applications in molecular spintronics [6]. Quantum manipulation of the spin in such materials can be envisioned provided they have sufficiently long spin relaxation (T_1) and dephasing times (T_2). A first step has been the study of coherent QTM, in which the tunneling rates are faster than the rate of decoherence [7, 8]. These studies provided a lower bound on T_2 of about 0.5 ns. In SMM crystals dipolar interactions may limit the dephasing time, making it necessary to work with dilute SMM ensembles [9–11] or even individual molecules. For instance, a recent study of dilute doped antiferromagnetic wheels demonstrated a phase relaxation time of several microseconds at 1.8 K [12].

The phase relaxation rate $\Gamma_2 = 1/T_2$ is generally much greater than the energy relaxation rate Γ . For instance, an upper bound on T_2 of 50 ns was found in dilute Ni₄ solutions at 130 GHz and 5.5 K, where energy relaxation, rather than dipolar or hyperfine interactions, may be the limiting mechanism [10]. Interestingly, the relaxation rate

Γ due to a direct spin-phonon process of a SMM embedded in an elastic medium can be derived without any unknown coupling constant [13, 14]. Moreover, collective relaxation effects are expected in SMM single crystals, such as phonon superradiance [15].

Direct measurements of the magnetization under pulse microwave (MW) irradiation enable study of spin-dynamics in SMM crystals [16–19]. In Fe₈, long pulses ($> 10 \mu\text{s}$) of resonant MW radiation drive spins and phonons out of equilibrium, and heating effects or phonon bottleneck (PB) preclude the observation of fast dynamics [16, 18]. However, using very short high power MW pulses, refs. [17] and [19] showed that these effects can be circumvented, enabling the observation of spin-dynamics on microsecond time scales. Ref. [17] explains the observed temperature dependence of the level lifetimes with direct spin-phonon coupling whereas ref. [19] concludes that a PB develops and plays an essential role in the magnetization dynamics.

Several experiments on SMM crystals in the quasi-static regime [20, 21] were explained based on the *ad hoc* model of PB [22, 23]. Only recently has this effect been investigated on microscopic basis [24, 25]. When N_S , the num-

ber of spins in a crystal, becomes comparable to N_{ph} , the number of resonant phonon modes (which can take energy out from the spin system), spin relaxation leads to the so-called bottleneck plateau [24]. Only because phonons themselves can relax to another reservoir is thermal equilibrium eventually attained. Hence, the collective dynamics of spins *plus* resonant phonons depends on phonon relaxation, which can be limited at low temperatures [26]. In SMM crystals the bottleneck parameter $B \equiv N_S/N_{\text{ph}}$ is very large ($\gg 10$), even though the resonant lines are broadened by inhomogeneities [25]. Hence, collective effects in spin-phonon relaxation should be strong in SMMs.

This Letter presents a study of magnetization relaxation in the SMM Ni_4 under steady state conditions of low amplitude and continuous microwave irradiation. The general methods used can be applied to any spin system, including other molecular magnets. A large transverse field is used to tune the energy splitting between the two lowest spin-states [8], while small deviations from equilibrium magnetization induced by a resonant MW field are monitored. Simultaneous measurements of the absorbed MW power and of the magnetization enable measurement of energy relaxation rate as a function of temperature. Experimental results are compared with detailed calculations of the relaxation rate between the first excited state and the ground state, using the density matrix equation (DME) with the relaxation terms in the universal form [13,14].

In steady state, the energy level populations are constant. Under continuous wave (cw) irradiation of frequency $f = \omega_0/(2\pi)$, the absorbed power P_{abs} is proportional to the spin-photon transition rate Λ and to the population difference $N_0 = N_a - N_b$ between the states $|a\rangle$ and $|b\rangle$ involved in the transition. The latter is reduced from its equilibrium value N_0^{eq} by the resonant perturbation. This reduction depends on the ratio between the transition and relaxation rates. For a two level system, the total relaxation rate is $\Gamma = \Gamma_{ab} + \Gamma_{ba}$ and $P_{\text{abs}} = \hbar\omega_0\Lambda N_0 = \hbar\omega_0\Lambda N_0^{\text{eq}}/(1 + 2\Lambda/\Gamma)$. Λ can be eliminated giving $\Gamma = 2P_{\text{abs}}/(\hbar\omega_0(N_0^{\text{eq}} - N_0))$. The populations can be obtained from magnetization measurement, $M = N_a m_a + N_b m_b = M^{\text{eq}} + \Delta M$. Thus the total relaxation rate between $|a\rangle$ and $|b\rangle$ can be expressed in terms of the measurable quantities P_{abs} and ΔM as follows:

$$\Gamma = \frac{(m_b - m_a) P_{\text{abs}}}{\Delta M \hbar\omega_0}. \quad (1)$$

Eq. (1) is a simple result of the balance between absorption and relaxation in steady state for a two level system. If the system has more than two levels – with levels a and b lowest in energy – one can still consider an effective two-level model in which relaxation between $|a\rangle$ and $|b\rangle$ is assisted by upper levels, provided that the temperature is sufficiently low so that the populations of all other levels are small. The use of eq. (1) is still justified because the upper levels do not contribute to P_{abs} and ΔM .

Simultaneous measurements of P_{abs} and ΔM have been previously used to measure relaxation times in paramag-

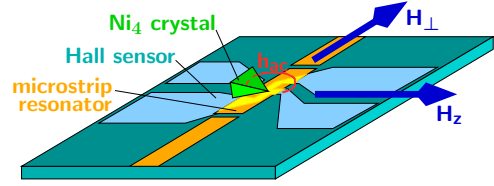


Figure 1: (Color online) Schematic of the integrated sensor used in this study.

nets and ferromagnets [27,28]. Recently, quantitative determination of the magnetization suppression under high power cw irradiation was obtained in the SMM Fe_8 using a commercial SQUID [29]. Here, we use a novel integrated sensor that incorporates a microstrip resonator with a micro-Hall magnetometer [30], which enables low power studies. Briefly, the Hall sensor is fabricated from a 2 dimensional electron gas in a GaAs/AlGaAs heterostructure. A microstrip resonator is capacitively coupled to two transmission lines and lithographically placed on the Hall sensor, as shown in fig. 1. A thin dielectric separates the resonator from the heterostructure material. The magnetometer, biased with a dc current of $10 \mu\text{A}$, permits detection of changes in the magnetization ΔM as small as 10^{-4} of the saturation magnetization M_s of our SMM crystals. The resonator has a fundamental resonance frequency of 10 GHz, for which the ac field h_{ac} is maximum at the sample location. This is also the case for the third harmonic, at 27.8 GHz. The large filling factor of the resonator enables the detection of absorbed power in the nW range for $\approx 100^3 \mu\text{m}^3$ samples. h_{ac} was calibrated at room temperature at each frequency through DPPH saturation. A vector network analyzer is used as a MW source and for transmission measurements. The integrated sensor is mounted in a ^3He cryostat with a base temperature of 0.37 K, in a superconducting vector magnet that enables magnetic fields to be applied in arbitrary directions with respect to the axes of the crystal.

$[\text{Ni}(\text{hmp})(\text{dmb})\text{Cl}]_4$ (Ni_4) is a particularly clean SMM with no solvate molecules present in its crystal phase and only 1% (natural abundance) of nuclear spins on the transition metal sites [31]. This results in narrower EPR peaks than in many SMMs [32]. The spin Hamiltonian of Ni_4 is to first approximation:

$$\hat{H}_S = -DS_z^2 - BS_z^4 + C(S_+^4 + S_-^4) - \mu_B \mathbf{H} \cdot \hat{\mathbf{g}} \cdot \mathbf{S}, \quad (2)$$

where the first term is the uniaxial anisotropy, the second and third terms are 4^{th} -order anisotropy terms, and the last term is the Zeeman energy. The $S = 4$ ground state of the molecule at low temperature is a consequence of ferromagnetic exchange interactions between the four Ni^{II} ($S = 1$) ions. The uniaxial anisotropy leads to a large energy barrier $DS^2 \approx 12 \text{ K}$ to magnetization reversal between states of projection $S_z = \pm 4$ along the easy axis of the molecule. The large C -term is at the origin of the fast tunneling ($\approx 10 \text{ MHz}$) observed at zero field [33] and

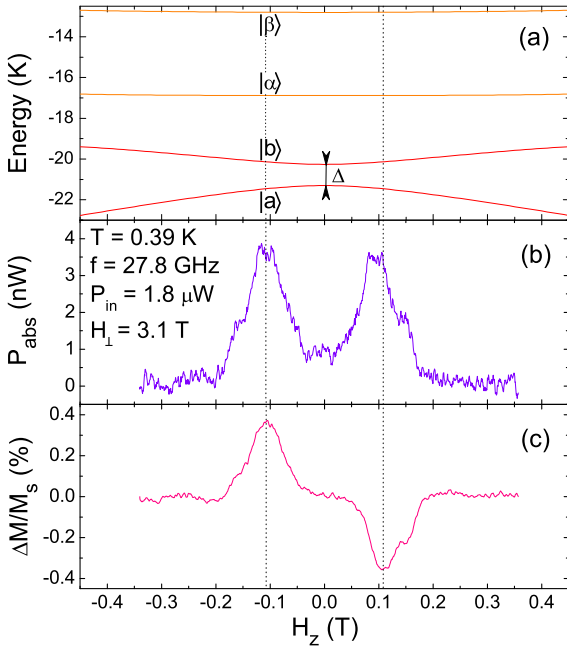


Figure 2: (Color online) (a) Energy levels of Ni₄ vs. longitudinal field H_z in the presence of a transverse field $H_{\perp} = 3.1$ T. (b) Absorbed power and (c) magnetization changes vs. H_z measured with an the integrated sensor as the Ni₄ crystal is irradiated at 27.8 GHz. The dashed vertical lines show the resonant transitions between the two lowest levels $|a\rangle$ and $|b\rangle$ corresponding to this frequency.

a recent analysis shows that the 4th-order terms in eq. (2) result from a finite ratio of the (second order) single ion anisotropies to exchange constant [34].

A pyramidal Ni₄ crystal containing $N_S = (7 \pm 0.5) \times 10^{14}$ molecules is affixed to the integrated sensor with vacuum grease and oriented so that h_{ac} is within 20° of z , the axis of the pyramid. A constant transverse field H_{\perp} is applied¹ perpendicularly to z , while the longitudinal field H_z is swept [8,30]. In this configuration, an avoided crossing between the two lowest energy levels $|a\rangle$ and $|b\rangle$ occurs, with a tunnel splitting Δ (fig. 2(a)). The energy levels and eigenstates are calculated by direct diagonalization of the Hamiltonian (eq. (2)). The character of the states $|a\rangle$ and $|b\rangle$ changes with H_z . At $H_z = 0$, they have zero magnetization along z . To have a measurable magnetization we work at finite H_z , where m_a and m_b are also finite and almost opposite. In the presence of cw MW irradiation, power absorption can be detected when the splitting between $|a\rangle$ and $|b\rangle$ matches the photon energy $\hbar\omega_0$ (fig. 2(b)). Simultaneous magnetization changes ΔM are observed (fig. 2(c))². By repeating this experiment at different transverse fields with the MW frequency fixed, it is possible to determine the zero

¹At an angle $\phi \simeq 11^\circ$ with the hard axis, estimated from the crystal geometry [33].

²Ni₄ molecules in a different molecular environment are responsible for the peak shoulders at $\approx \pm 0.15$ T [32].

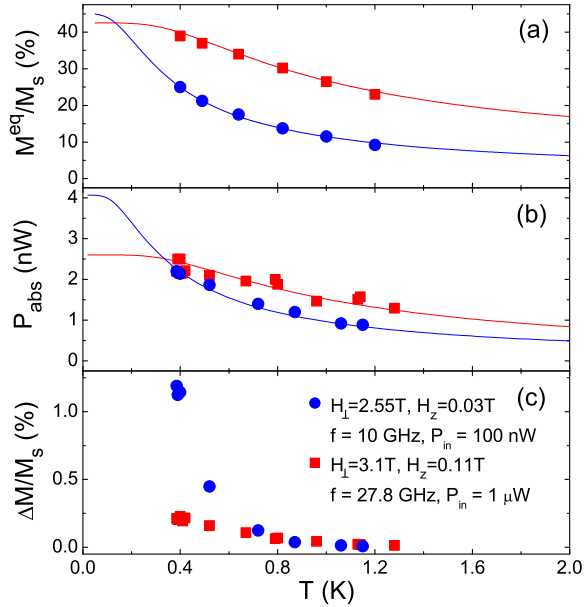


Figure 3: (Color online) (a) Equilibrium magnetization, (b) absorbed power and (c) magnetization changes vs. temperature, measured for two values of the applied field, corresponding to transition frequencies of 10 and 27.8 GHz. The continuous lines are calculations (see text).

field splitting parameters [8,30], which are found to be in good agreement with those deduced from high frequency EPR experiments [32,33]. Using the two frequencies available for our microstrip resonator, we obtain $D = 0.75$ K, $B = 7 \times 10^{-3}$ K, $C = 2.9 \times 10^{-4}$ K, $g_x = g_y = 2.23$ and $g_z = 2.3$.

We now concentrate on the behavior of P_{abs} and ΔM vs. temperature for two values of the applied field (fig. 3). $(H_{\perp}, H_z)_1 = (2.55, 0.03)$ T corresponds to a transition frequency of 10 GHz and $(H_{\perp}, H_z)_2 = (3.1, 0.11)$ T to 27.8 GHz. In both cases, only the two lowest-lying states are significantly populated within the temperature range investigated. At 1.5 K, less than 3% of the molecules occupy other states. The first such state lies several Kelvins above b (see fig. 2(a)), and thus the effective two-state model discussed above is valid. The temperature dependence of the equilibrium magnetization in the absence of MW, M^{eq} , is plotted in fig. 3(a). It is well reproduced by the two-state model (continuous lines):

$$\frac{M^{\text{eq}}}{M_s} = \frac{m_a + m_b \exp(-\hbar\omega_0/(k_B T))}{S(1 + \exp(-\hbar\omega_0/(k_B T)))}, \quad (3)$$

where m_a , m_b and ω_0 are calculated from diagonalization of \hat{H}_S . It is found that $m_a/S = 0.45$ and $m_b/S = -0.432$ for $(H_{\perp}, H_z)_1$, and that $m_a/S = 0.425$ and $m_b/S = -0.329$ for $(H_{\perp}, H_z)_2$.

When irradiating the sample with MW, the power was deliberately kept small in order to investigate small deviations from equilibrium, typically less than 1%. The lowest achievable sample temperature under these conditions is

0.385 K, only 15 mK above the cryostat base temperature. The measured temperature dependence of P_{abs} is plotted in fig. 3(b) together with the formula:

$$P_{\text{abs}} = \hbar\omega_0 \left(\frac{g\mu_B}{\hbar} h_{\text{ac}} \right)^2 \frac{| \langle a | S_z | b \rangle |^2}{2\Gamma_2^*} N_S \tanh \left(\frac{\hbar\omega_0}{2k_B T} \right). \quad (4)$$

Γ_2^* is an upper bound on the dephasing rate, and can be extracted from the line width, found to be about 4 GHz [30]. The only fitting parameter for the continuous lines displayed in fig. 3(b) is h_{ac} , which is found to be 1.9 mOe at 10 GHz and 1.3 mOe at 27.8 GHz. These values are 30 to 50% less than expected from calibration. The difference in the temperature dependences of M^{eq} and P_{abs} under the different applied fields is simply due to the different level splittings, $\hbar\omega_0$, in the Boltzmann factors of eqs. (3) and (4). Finally ΔM , the magnetization change induced by the MW absorption, is plotted in fig. 3(c) for the two applied fields. Its temperature dependence is much stronger than that of M^{eq} and P_{abs} . $\Delta M/M_s$ decreases by almost two orders of magnitude at 10 GHz as T increases from 0.385 to 1.2 K, and by almost a factor 20 at 27.8 GHz.

With the data presented in fig. 3 and eq. (1) we have extracted³ the energy relaxation rate Γ . It is displayed in a semilog plot vs. the inverse temperature $1/T$ in fig. 4. The general trend of the data at 10 and 27.8 GHz is a moderate increase of Γ with temperature at low temperatures ($T < 0.8$ K) followed by an exponential growth at higher temperatures.

A direct spin-phonon relaxation process from $|b\rangle$ to $|a\rangle$ is not consistent with the data, because it would lead to a more gradual temperature dependence of the relaxation rate. In the case where the transverse field is mainly responsible for the energy splitting between states, it reads [14],

$$\Gamma_{\text{sp},T} = \frac{1}{2} Q S^2 \frac{\Delta^2 \omega_0 (g\mu_B H_{\perp})^2}{12\pi E_t^4} \coth \left(\frac{\hbar\omega_0}{2k_B T} \right), \quad (5)$$

where $Q \cong 1$ when $SH_z < H_{\perp}$ and $E_t = (\rho v_t^5 \hbar^3)^{1/4}$ is the characteristic energy of the spin-phonon interaction. ρ is the density of Ni_4 , and v_t the speed of the transverse phonons. The temperature dependence of $\Gamma_{\text{sp},T}$ is much weaker than that of the measured rate Γ , even at low temperature. The zero temperature spin-phonon relaxation rate Γ_{sp} given by the prefactor of eq. (5) is very sensitive to the precise value of the transverse speed of sound, since v_t appears to the fifth power. The latter was extracted from the heat capacity $C(T)$ of Ni_4 [35] using the extended Debye model [36]. The soft phonon mode, $v_t = 940$ m/s, is nearly transverse and the most important for the spin-phonon relaxation, whereas the two stiff modes with $v = 2250$ m/s can be neglected. The prefactor $\frac{1}{2}$ in eq. (5) accounts for the fact that only one phonon mode contributes to the spin-phonon process. Using the

³In order to extract Γ up to $T = 1.6$ K, the 10 GHz data of fig. 4 also include measurements at a MW power of $P_{\text{in}} = 1 \mu\text{W}$.

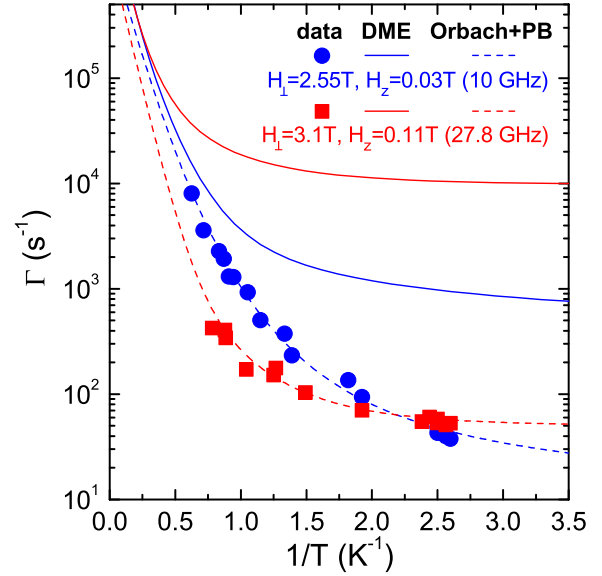


Figure 4: (Color online) Dependence of the energy relaxation rate at 10 and 27.8 GHz on inverse temperature deduced from the simultaneous measurements of fig. 3 and from eq. (1). The continuous lines are calculations using the universal DME and the dashed lines are fits of the data including the Orbach mechanism and PB (see text).

density of Ni_4 , $\rho = 1.4 \text{ g/cm}^3$ [37], we obtain $E_t = 75.7$ K. Using this value in eq. (5), the expected zero temperature relaxation rate from the direct process is found to be 40 and 200 times larger than the observed rate at 10 GHz and 27.8 GHz, respectively. Such a large disagreement can not be assigned to an uncertainty of v_t , which would have to differ by a factor 2 to 3 from the value we have taken. Also processes other than rotation of magnetic molecules without distortion, unaccounted for in the universal form of the spin-phonon coupling, cannot explain the discrepancy since they can only increase the relaxation rate.

This suggests that a PB is necessary to explain the data. In fact, an excellent agreement with the data at each frequency is obtained with the form of relaxation rate that combines PB and Orbach mechanism (see dashed lines in fig. 4):

$$\Gamma_T = \frac{\Gamma_{\text{ph}}}{B_{\omega_0}} \coth^2 \left(\frac{\hbar\omega_0}{2k_B T} \right) + \sum_i \Gamma_{0i} \exp \left(\frac{-E_i}{k_B T} \right). \quad (6)$$

This temperature dependence of the relaxation rate has also been observed in dilute paramagnetic salts [38].

The temperature dependence of the PB mechanism in the presence of phonon relaxation Γ_{ph} can be obtained from eqs. (60) of ref. [24] by including a large inhomogeneous broadening, as done in ref. [25]. In that case, the bottleneck parameter has the form:

$$B_{\omega_0} \equiv \frac{N_S \rho_S(\omega_0)}{N \rho_{\text{ph}}(\omega_0)} = \frac{N_S}{N \sqrt{2\pi}} \frac{2\pi^2 \tilde{\Omega}_D^3}{\omega_0^2 \delta\omega_0}. \quad (7)$$

Here, the spin density of states $\rho_S(\omega_0)$ is assumed to have a

Gaussian line shape of width $\delta\omega_0$, N is the number of unit-cells and v_0 their volume. $\tilde{\Omega}_D = v_t/v_0^{1/3}$ is proportional to the Debye frequency. Integrating out $r_{\mathbf{k}}$ and then over the narrow natural line shape in eqs. (60) of ref. [24] with the added inhomogeneous broadening leads to equations:

$$\begin{aligned}\dot{p}_{\omega_0} &= -\Gamma_{\text{sp}} [p_{\omega_0} + (2p_{\omega_0} - 1)n_{\omega_0}] \\ \dot{n}_{\omega_0} &= \Gamma_{\text{ph}} (n_{\omega_0}^{\text{eq}} - n_{\omega_0}) - B_{\omega_0}\dot{p}_{\omega_0},\end{aligned}\quad (8)$$

that are similar to those of refs [22, 23]. p_{ω_0} is the population of the spin's excited state and n_{ω_0} the phonon population. From linearization of eqs. (8) for $B_{\omega_0} \gg 1$, it can be found that the lowest rate governing the relaxation is:

$$\Lambda_- \cong \frac{\Gamma_{\text{ph}}\Gamma_{\text{sp},T}}{B_{\omega_0,T}\Gamma_{\text{sp},T} + \Gamma_{\text{ph}}},\quad (9)$$

where $B_{\omega_0,T} = B_{\omega_0} \tanh^2(\hbar\omega_0/(2k_B T))$. In the strong bottleneck limit, $\Gamma_{\text{ph}} \ll B_{\omega_0,T}\Gamma_{\text{sp},T}$, the so-called bottleneck rate $\Lambda_- \cong \Gamma_{\text{b}} = \Gamma_{\text{ph}}/B_{\omega_0,T}$ dominates, as in our experiments at low temperature, *i.e.*, the first term of eq. (6). In Ni₄, the unit-cell contains four molecules and its volume is $v_0 = 5777.1 \text{ \AA}^3$ [37]. Hence, $N_S/N = 4$ and $\tilde{\Omega}_D = 8.3 \times 10^{11} \text{ s}^{-1}$. Using $\delta\omega_0 = 25 \times 10^9 \text{ s}^{-1}$, $B_{\omega_0} \approx 180000$ at 10 GHz and $B_{\omega_0} \approx 24000$ at 27.8 GHz, values which also depend strongly on v_t . From the prefactors of the PB mechanism used to fit the data (see dashed lines on fig. 4), we find that in our experiments, the phonon relaxation time $T_{\text{ph}} = 1/\Gamma_{\text{ph}} \approx 0.4 \text{ \mu s}$ at 10 GHz and $\approx 0.8 \text{ \mu s}$ at 27.8 GHz. This corresponds to a phonon mean free path of about 500 μm , for a crystal whose largest dimension is 180 μm . These values are comparable to published ones [23], and reveal that the phonons undergo several reflections on the crystal walls before escaping.

To better understand the relaxation including the Orbach mechanism that contributes to eq. (6), we have performed calculations of the relaxation rate between the two lowest-lying states in the whole temperature range, using the density matrix equation (DME) with the relaxation terms in the universal form [13, 14]. In this approach, the complete set of energy levels and the effect of temperature are taken into account. The explicit form of the crystal fields enters through the eigenfunctions and eigenvalues of the Hamiltonian (eq. (2)) that are universal building blocks of the relaxation term of the DME. This makes inclusion of various anisotropies easy since it does not change the structure of the latter. The continuous lines in fig. 4 are the results of DME calculations for the applied fields $(H_{\perp}, H_z)_1$ and $(H_{\perp}, H_z)_2$ used in the experiments. The Hamiltonian parameters and characteristic energy of the spin-phonon coupling needed for the calculation are the same as given above. The low temperature part of the DME calculations corresponds to the direct spin-phonon process, which is given by eq. (5). As previously explained, this process is screened out by PB. The calculated relaxation rate follows the direct process until the temperature reaches about 0.8 K. Above this temperature, an exponential growth of the rate is observed. This behavior would

level i	3	4	5
10 GHz, E_i (K)	3.27	6.45	10.61
Γ_{0i}^{DME} (s^{-1})	1.7×10^4	5×10^5	1.5×10^6
Γ_{0i}^{fit} (s^{-1})	10^4	2.5×10^5	1.5×10^6
27.8 GHz, E_i (K)	3.25	7.34	12.28
Γ_{0i}^{DME} (s^{-1})	3.5×10^4	7×10^5	1.5×10^6
Γ_{0i}^{fit} (s^{-1})	2×10^3	5×10^4	1.5×10^6

Table 1: Levels involved in the Orbach mechanism for the two studied frequencies. The calculated strengths using DME as well as the fitted values to the data are summarized.

not be expected for a pure two-level system. But within the giant spin approximation, the $S = 4$ Ni₄ SMM has seven other levels lying above the two lowest ones, $|a\rangle$ and $|b\rangle$. Two of them, $|\alpha\rangle$ and $|\beta\rangle$, have been represented in fig. 2(a). Although they are weakly populated within the temperature range investigated, their presence can greatly enhance the relaxation rate. Instead of the direct relaxation $|b\rangle \rightarrow |a\rangle$, the system can be thermally excited from $|b\rangle$ to some high level, say $|i\rangle$, and then fall down to $|a\rangle$. This is the Orbach mechanism, yielding a characteristic Arrhenius temperature dependence of the rate, *i.e.*, the second term of eq. (6). Its activation energy E_i equals the separation between levels b and i , whereas its strength Γ_{0i} depends on the coupling between $|i\rangle$ and $|a\rangle$ through transverse phonons.

From the same statistical argument mentioned in the introduction, the Orbach mechanism can also be bottlenecked. But the emitted phonons have a much higher frequency E_i/h than those from the direct process, leading to a much lower bottleneck parameter (*i.e.*, there is a much higher density of phonon modes available for spin relaxation). Assuming the same inhomogeneous broadening $\delta\omega_0$, $B_{\omega_0} \approx 800$ for $E_i = 7 \text{ K}$, which is close to the energy separation between $|b\rangle$ and the fourth energy level for the two different applied fields. Assuming that Γ_{ph} is independent of temperature, only processes with a rate larger than about $5 \times 10^3 \text{ s}^{-1}$ will be strongly bottlenecked (eq. (9)). This can be seen from the data, which behave differently at 10 and at 27.8 GHz in the high temperature region of fig. (4). Whereas the measured rate at 27.8 GHz is still two orders of magnitude lower than the calculated one, the data at 10 GHz tend to meet the DME calculation. This is due to the fact that as the Orbach mechanism starts, the rate computed at 10 GHz using the universal DME is still low ($\Gamma \approx 10^3 - 10^4 \text{ s}^{-1}$), and hence weakly bottlenecked. On the contrary, the relaxation at 27.8 GHz is still strongly bottlenecked in that temperature range because the calculated rate is faster than 10^4 s^{-1} . Table 1 summarizes the three Orbach channels relevant for the energy relaxation in the temperature range studied. It gives their activation energies, their calculated strengths using DME, and the values fitted to the data using eq. (6). The fitted values are smaller than the calculated ones because

PB is not completely suppressed. As explained, this effect is stronger at 27.8 GHz than at 10 GHz.

It is interesting to estimate the phonon relaxation rate necessary to suppress the PB from eq. (9). If the phonon relaxation is very fast, $B_{\omega_0, T} \Gamma_{sp, T} \ll \Gamma_{ph}$, $\Lambda_- \cong \Gamma_{sp, T}$, and there is no bottleneck. One would need to have $T_{ph} \ll 10$ ns at 10 GHz and $T_{ph} \ll 4$ ns at 27.8 GHz to meet this requirement at low temperature. This would only be possible for a submicron-size crystal.

In conclusion, the temperature dependence of the energy relaxation rate between the two lowest-lying spin-states of Ni₄ has been measured at two different frequencies. Using calculations of the rate based on the universal DME and taking into account PB that screens out the direct spin-phonon process at low temperature, the two sets of data are well accounted for in the whole temperature range investigated. In particular, the Orbach mechanism dominates at high temperatures, and is weakly bottlenecked at 10 GHz. Finally, we point out that the fact that the universal DME calculations and the PB work so well to explain the data is surprising, as coherence is expected to play an important role in collective spin-lattice relaxation in SMM crystals [15, 39].

This work was supported by NSF Grants No. DMR-0506946 and DMR-0703639. We acknowledge E. DEL BARCO, S. HILL and E. M. CHUDNOVSKY for useful discussions.

References

- [1] FRIEDMAN J. R., SARACHIK M. P., TEJADA J. and ZIOLO R., *Phys. Rev. Lett.*, **76** (1996) 3830.
- [2] THOMAS L., LIONTI F., BALLOU R., GATTESCHI D., SESSOLI R. and BARBARA B., *Nature*, **383** (1996) 145.
- [3] WERNSDORFER W. and SESSOLI R., *Science*, **284** (1999) 133.
- [4] RAMSEY C. M., DEL BARCO E., HILL S., SHAH S. J., BEEDLE C. C. and HENDRICKSON D. N., *Nature Physics*, **4** (2008) 277.
- [5] LEUENBERGER M. N. and LOSS D., *Nature*, **410** (2001) 789.
- [6] BOGANI L. and WERNSDORFER W., *Nature Materials*, **7** (2008) 179.
- [7] HILL S., EDWARDS R. S., ALIAGA-ALCALDE N. and CHRISTOU G., *Science*, **302** (2003) 1015.
- [8] DEL BARCO E., KENT A. D., YANG E. C. and HENDRICKSON D. N., *Phys. Rev. Lett.*, **93** (2004) 157202.
- [9] HALLAK F. E., VAN SLAGEREN J., GOMEZ-SEGURA J., RUIZ-MOLINA D. and DRESSEL M., *Phys. Rev. B*, **75** (2007) 104403.
- [10] DE LOUBENS G., KENT A. D., KRYMOV V., GERFEN G. J., BEEDLE C. C. and HENDRICKSON D. N., *J. Appl. Phys.*, **103** (2008) 07B910.
- [11] HENDERSON J. J., RAMSEY C. M., DATTA S., DEL BARCO E., HILL S., STAMATATOS T. C. and CHRISTOU G., in preparation.
- [12] ARDAVAN A., RIVAL O., MORTON J. J. L., BLUNDELL S. J., TYRYSHKIN A. M., TIMCO G. A. and WINPENNY R. E. P., *Phys. Rev. Lett.*, **98** (2007) 057201.
- [13] CHUDNOVSKY E. M., *Phys. Rev. Lett.*, **92** (2004) 120405.
- [14] CHUDNOVSKY E. M., GARANIN D. A. and SCHILLING R., *Phys. Rev. B*, **72** (2005) 094426.
- [15] CHUDNOVSKY E. M. and GARANIN D. A., *Phys. Rev. Lett.*, **93** (2004) 257205.
- [16] PETUKHOV K., BAHR S., WERNSDORFER W., BARRA A.-L. and MOSSER V., *Phys. Rev. B*, **75** (2007) 064408.
- [17] BAHR S., PETUKHOV K., MOSSER V. and WERNSDORFER W., *Phys. Rev. B*, **77** (2008) 064404.
- [18] BAL M., FRIEDMAN J. R., RUMBERGER E. M., SHAH S., HENDRICKSON D. N., AVRAHAM N., MYASOEDOV Y., SHTRIKMAN H. and ZELDOV E., *J. Appl. Phys.*, **99** (2006) 08D103.
- [19] BAL M., FRIEDMAN J. R., CHEN W., TUOMINEN M. T., BEEDLE C. C., RUMBERGER E. M. and HENDRICKSON D. N., *Europhys. Lett.*, **82** (2008) 17005.
- [20] CHIORESCU I., WERNSDORFER W., MULLER A., BOGGE H. and BARBARA B., *Phys. Rev. Lett.*, **84** (2000) 3454.
- [21] SCHENKER R., LEUENBERGER M. N., CHABOUSSANT G., LOSS D. and GUEDEL H. U., *Phys. Rev. B*, **72** (2005) 184403.
- [22] FAUGHNAN B. W. and STRANDBERG M. W. P., *J. Phys. Chem. Solids*, **19** (1961) 155.
- [23] SCOTT P. L. and JEFFRIES C. D., *Phys. Rev.*, **127** (1962) 32.
- [24] GARANIN D. A., *Phys. Rev. B*, **75** (2007) 094409.
- [25] GARANIN D. A., *Phys. Rev. B*, **77** (2008) 024429.
- [26] LOUNASMAA O. V., *Experimental principles and methods below 1 K* (Academic Press, London & New York) 1974.
- [27] BLOEMBERGEN N. and WANG S., *Phys. Rev.*, **93** (1954) 72.
- [28] DE LOUBENS G., NALETOV V. V. and KLEIN O., *Phys. Rev. B*, **71** (2005) 180411(R).
- [29] CAGE B., RUSSEK S. E., ZIPSE D., NORTH J. M. and DALAL N. S., *Appl. Phys. Lett.*, **87** (2005) 082501.
- [30] DE LOUBENS G., CHAVES-O'FLYNN G. D., KENT A. D., RAMSEY C., DEL BARCO E., BEEDLE C. C. and HENDRICKSON D. N., *J. Appl. Phys.*, **101** (2007) 09E104.
- [31] YANG E.-C., WERNSDORFER W., HILL S., EDWARDS R. S., NAKANO M., MACCAGNANO S., ZAKHAROV L. N., RHEINGOLD A. L., CHRISTOU G. and HENDRICKSON D. N., *Polyhedron*, **22** (2003) 1727.
- [32] EDWARDS R. S., MACCAGNANO S., YANG E.-C., HILL S., WERNSDORFER W., HENDRICKSON D. N. and CHRISTOU G., *Journ. Appl. Phys.*, **93** (2003) 7807.
- [33] KIRMAN C., LAWRENCE J., HILL S., YANG E.-C. and HENDRICKSON D. N., *J. Appl. Phys.*, **97** (2005) 10M501.
- [34] WILSON A., LAWRENCE J., YANG E.-C., NAKANO M., HENDRICKSON D. N. and HILL S., *Phys. Rev. B*, **74** (2006) 140403.
- [35] HENDRICKSON D. N. *et al.*, *Polyhedron*, **24** (2005) 2280.
- [36] GARANIN D. A., *arXiv:0804.1066v3*, (2008) .
- [37] YANG E.-C. *et al.*, *Inorg. Chem.*, **45** (2006) 529.
- [38] RUBY R. H., BENOIT H. and JEFFRIES C. D., *Phys. Rev.*, **127** (1962) 51.
- [39] CALERO C., CHUDNOVSKY E. M. and GARANIN D. A., *Phys. Rev. B*, **76** (2007) 094419.